IEEE Access
Multidisciplinary | Rapid Review | Open Access Journal

Received October 5, 2020, accepted November 5, 2020, date of publication November 10, 2020, date of current version November 23, 2020.

*Digital Object Identifier 10.1109/ACCESS.2020.3037216*

# Dynamic Hysteresis Model and Control Methodology for Force Output Using Piezoelectric Actuator Driving

**JIAN CHEN, GUOXIANG PENG, HONG HU, (Member, IEEE), AND JIA NING**
School of Mechanical Engineering and Automation, Harbin Institute of Technology, Shenzhen 518055, China

Corresponding author: Hong Hu (honghu@hit.edu.cn)

This work was supported by the Shenzhen Government Fund under Grant JCY20170413105740689 and Grant JSGG20170412143346791.

**ABSTRACT** In the application of piezoelectric jet dispensing, piezoelectric ceramics and flexure hinges cooperate to form a piezoelectric actuator. The dispensing quality of the piezoelectric jet is closely associated with the output force of the piezoelectric actuator. In this study, a corresponding piezoelectric actuator output force experiment platform is built, and the voltage-force hysteresis curve of the piezoelectric actuator is analyzed. The voltage-force hysteresis curve exhibits memory characteristics and rate dependence. A modeling method for the dynamic hysteresis output force model is proposed, and the numerical method of the model is presented. The corresponding output force model of the piezoelectric actuator is established based on experimental data to predict the output force under different input voltages. According to the dynamic hysteresis model, the feedforward control methodology of the dynamic hysteresis inverse model is proposed, and experimental tests are performed. Experimental results show that the proposed model can express the complex nonlinear characteristics of piezoelectric actuators, and the output force feedforward control method based on the dynamic hysteresis inverse model effectively decreases the nonlinear characteristics of the piezoelectric actuator.

**INDEX TERMS** Piezoelectric actuator, force control, Preisach model, dynamic hysteresis.

## I. INTRODUCTION

Piezoelectric ceramics exhibit characteristics of rapid response, small size, high working bandwidth, and micro-nano-level positioning accuracy. Therefore, they are widely used in parts of high-precision positioning systems, such as those for adjusting the nanometer distance between probes and samples in atomic force microscopes [1]; for realizing micro-nano-level material manipulation and movement in micromanipulators [2], inchworm linear motors [3], and inertial motors [4]; and for ultraprecision machining [5]. Furthermore, piezoelectric ceramics can be used as liquid jet drivers owing to their fast response speed. Huang *et al.* [6], used piezoelectric ceramics to create a universal piezoelectric-driven ultrasonic cell microinjection system. Khalate *et al.* [7], used piezoelectric ceramics to achieve on-demand ink titration. However, owing to vibration, hysteresis [8], and creep [9], the nonlinear characteristics of piezoelectric ceramics significantly reduce the control accuracy of a piezoelectric actuator, which is a typical nonlinear system that cannot be easily controlled using linear system control methods.

The piezoelectric ceramic control method generally requires a mathematical model to describe the hysteresis of piezoelectric ceramics and then obtain a hysteresis inverse model to complete their feedforward control. Piezoelectric ceramics can be modeled using various methods, which are mainly categorized into modeling methods based on hysteresis operators, differential equation models, and other mathematical modeling methods. The dynamic hysteresis of piezoelectric ceramics demands substantial requirements for the modeling method of piezoelectric ceramics. The hysteresis of piezoelectric ceramics can be expressed at different frequencies. Yu *et al.* [10] introduced the derivative of voltage with time and created a new density function to associate the dynamic Preisach model (DPM) with the classical Preisach model (CPM), completing the dynamic hysteresis modeling of the output displacement of piezoelectric

The associate editor coordinating the review of this manuscript and approving it for publication was Feiqi Deng.

ceramics. Based on the traditional Prandtl-Ishlinskii model, Janaideh *et al.* [11] introduced dynamic functions related to voltage and frequency to an input and hysteresis operator, thereby completing a rate-dependent model that can describe the dynamic hysteresis. Modeling methods based on differential equations, such as the Duhem model [12] and Bouc-Wen model [13], have been proposed; however, these methods cannot easily obtain general solutions of differential equation models. In addition, other mathematical models exist for the voltage-displacement dynamic hysteresis modeling of piezoelectric ceramics, such as that by Gu *et al.* [14], which is based on the shape of the hysteresis loop, involving the maximum height of the hysteresis loop, distance of the hysteresis curve, hysteresis loop rotation angle, and other parameters. A set of elliptic curves are used to characterize the dynamic hysteresis of piezoelectric ceramics, and the inverse of the ellipse model for feedforward control can be obtained easily. Cheng *et al.* [15] established a hysteresis sub-model and a dynamic sub-model through a multilayer fully-connected neural network; subsequently, two neural networks were used to identify the complex dynamic hysteresis, and the dynamic hysteresis modeling of piezoelectric ceramics was completed.

Although extensive research has been conducted regarding the position control of piezoelectric ceramics [16], few studies have addressed their output force control. The active variable damping vibration control of robot joints [17] is affected by the output force of piezoelectric ceramics and the stability of the output force. The hysteresis model and output force prediction method of the piezoelectric actuator have been used to solve some of the output force control problems of the piezoelectric actuator. A statistical model based on the output force was compensated by a discrete P-I feedback controller [18], and a force detector based on the hyperbolic model was used for PID feedback control [19]. In the application of piezoelectric jet dispensing valves [20], [21], the output displacement of piezoelectric ceramics often cannot satisfy travel requirements, as piezoelectric ceramics typically form a piezoelectric actuator with a lever-type flexure hinge or a straight circular flexure hinge. The output displacement of the piezoelectric actuator is often fixed, which does not significantly affect the dispensing quality; however, the output force of the piezoelectric actuator does significantly affect the dispensing quality. Moreover, different output force requirements exist for colloids of different viscosities. Piezoelectric ceramics are the core driving element of the piezoelectric actuator, and their nonlinear characteristics cause undesired results in the output force of the piezoelectric actuator.

To solve the output force control problem of the piezoelectric actuator, its voltage-force curve was investigated in this study. Consequently, it was discovered that the voltage-force curve was the same as the hysteresis curve, and that it possessed memory characteristics and rate dependence. Based on the classic Preisach model, the dynamic term is introduced, a dynamic hysteresis model is proposed, and a numerical method for the dynamic hysteresis model is proposed herein. The voltage-force data of the piezoelectric actuator were obtained experimentally to establish the piezoelectric actuator's output force model. According to the dynamic hysteresis model, a dynamic inverse model is proposed to calculate the compensation voltage for feedforward control to decrease the nonlinear characteristics of the piezoelectric actuator. Section 2 mainly introduces the construction of the experimental platform, experimental conditions, and analysis of the voltage-force nonlinear relationship of the piezoelectric actuator. Section 3 introduces the dynamic hysteresis model, numerical method of the dynamic hysteresis model, identification and modeling process, and the dynamic hysteresis model used to predict the output force of the piezoelectric actuator. In Section 4, the feedforward control method based on the dynamic hysteresis inverse model is introduced, and the experimental results of the output force tracking control of the piezoelectric actuator are analyzed.

## II. VOLTAGE-FORCE HYSTERESIS EXPERIMENTS

### A. EXPERIMENTAL PLATFORM

Before introducing the modeling methodology, it is necessary to analyze the voltage-force hysteresis of the piezoelectric actuator. The experimental process is shown in Fig. 1. The host computer controls the data acquisition card to provide an analog output signal $u(t)$ through the voltage amplifier, and the amplified signal $v(t)$ excites the piezoelectric ceramics. The flexible hinge amplifies the small displacement of the piezoelectric ceramics in the horizontal direction to the vertical direction. Simultaneously, the piezoelectric force sensor is squeezed by the piezoelectric actuator to generate a charge signal $q(t)$. The charge signal is converted into an output force signal $n(t)$ by the charge amplifier. The data acquisition card synchronously collects the input voltage signal $v(t)$ and output force signal $n(t)$. The dual-channel synchronous acquisition signal is used to analyze the voltage-force curve of the piezoelectric actuator.

The specific equipment configuration parameters of the experimental platform are as follows: LabVIEW was used to write data acquisition programs and control algorithm programs, and complete the control interface design. The data acquisition card uses an NI PXI6251 data acquisition card, which has high-speed synchronous analog input channels, analog output channels, and a 16-bit high-speed A/D, D/A converter. The voltage amplifier was an ATA-308 power amplifier manufactured by Antai Electronics Company, the force sensor was a SINOCERA CL-YD-303 piezoelectric force sensor, and the sensor bandwidth was 10 kHz. The stack driver was the P-887.91 model of PI Company, with a nominal displacement of 32 $\mu$m and a driving voltage of 0-120 V. The flexible hinge was self-designed [22]. After setting up the experimental platform, to protect the normal operation of the piezoelectric driver and ensure the stability of the experimental conditions, a pre-tightening force of 500 N was imposed on the piezoelectric ceramic and the flexible hinge. The pre-tightening force at both ends of the flexible hinge was approximately 200 N.

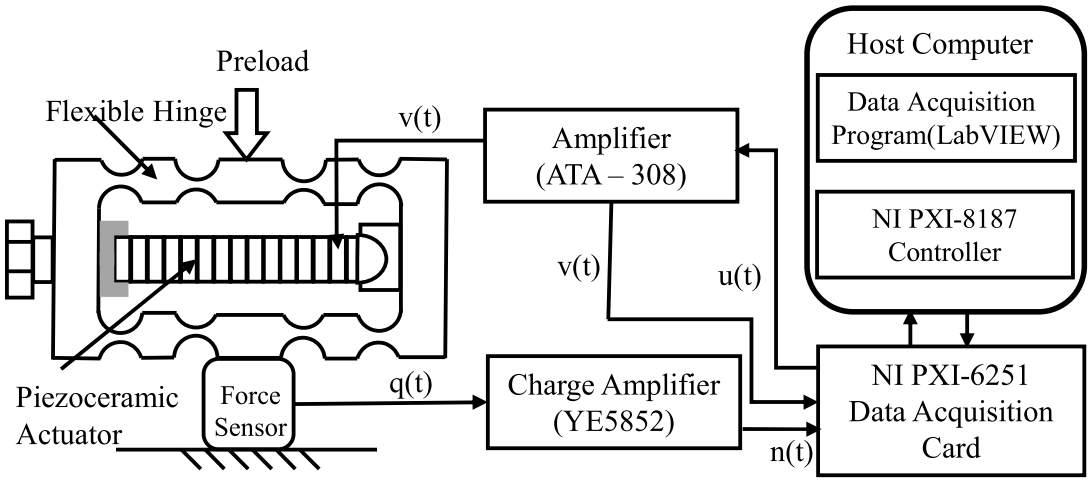


**FIGURE 1.** Piezoelectric actuator output force experimental platform.

### B. VOLTAGE-FORCE HYSTERESIS

Although piezoelectric ceramics exhibit characteristics of fast response speed, small size, and high accuracy, they also exhibit nonlinear characteristics that affect the control accuracy of piezoelectric actuators and reduce the stability of the control system. The nonlinear characteristics of piezoelectric actuators are mainly due to hysteresis, creep, and vibration, among which hysteresis is dominant in typical working conditions. The voltage-force curve of the piezoelectric actuator can be easily obtained using the experimental platform. It was discovered that the hysteresis in the piezoelectric actuator was not only reflected in the voltage-displacement relationship, but also in the voltage-force relationship. The output force is related not only to the current value of the input voltage, but also to the extreme value before the input voltage. This phenomenon is known as the memory characteristic of hysteresis. The input voltage was an attenuated sine wave, and the relationship between the input voltage and output force is shown in Fig. 2(a). The voltage-force curve in the figure shows multiple hysteresis loops. The rising curve does not coincide with the falling voltage curve. This shows that the output force hysteresis of the piezoelectric actuator exhibits a multi-value-mapping relationship; furthermore, it is related to the previous historical extreme values and possesses memory characteristics. The input voltage was an 80 V sine wave with different frequencies.The voltage-force curve under different excitation frequencies is shown in Fig. 2(b).Piezoelectric force sensor usually suffers from limited sensing accuracy at low frequencies, the minimum input frequency of the experiment is 20 Hz. When the frequency of the input voltage was 20 Hz, the hysteresis main loop, i.e., the difference between the voltage rise and fall curves, was the smallest. When the frequency of the input voltage was 300 Hz, the width of the hysteresis loop widened, and the maximum output force decreased, indicating that the voltage-force curve remained stable as the frequency of the excitation voltage changed, and that the hysteresis of the piezoelectric actuator was frequency dependent. This frequency-dependent hysteresis is known as dynamic hysteresis.

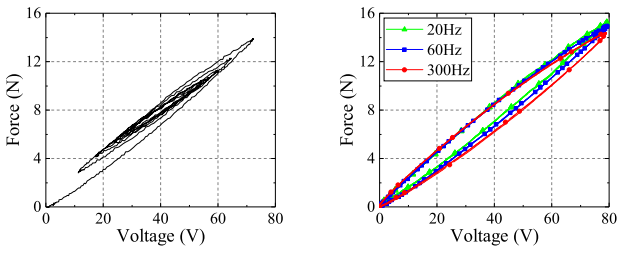


(a) Voltage–force hysteresis curve (b) Dynamic hysteresis

**FIGURE 2.** Hysteresis of output force of piezoelectric actuator.

## III. OUTPUT FORCE MODEL OF PIEZOELECTRIC ACTUATOR BASED ON DYNAMIC HYSTERESIS MODEL

### A. NUMERICAL METHOD OF DYNAMIC HYSTERESIS MODEL

Based on the experiment described in Section 2, the hysteresis of the piezoelectric actuator output force is rate dependent, whereas the classic Preisach model is a rate-independent hysteresis model. When the frequency spectrum of the input signal is complex, the classic Preisach model cannot accurately simulate the hysteresis, thereby further affecting the accuracy of the feedforward controller based on the inverse model. Therefore, based on the classic Preisach model, a dynamic hysteresis model is proposed herein to model the nonlinear characteristics of the piezoelectric actuator output force. Assume a set of input signals, where the local extreme value sequence of the input signal is $U = \{u(t_0), u(t_1) \cdots u(t_{2\,i}), u(t_{2\,i+1}) \cdots u(t)\}$. The odd-numbered term in the extreme value sequence is the local maximum, whereas the even-numbered term is the local minimum. The dynamic hysteresis model [23] can be expressed

as shown in (1).

$$F(t) = \sum_{i=0}^{w} \iint_{A[u(t_{2i}),u(t_{2i+1})]} \mu(\alpha, \beta) d\alpha d\beta - \sum_{i=0}^{l} \iint_{A[u(t_{2i+1}),u(t_{2i+2})]} \mu(\alpha, \beta) d\alpha d\beta \quad (1)$$

where, $F(t)$ represents the output value of the dynamic hysteresis model. $A\left[u\left(t_{2\,i}\right), u\left(t_{2\,i+1}\right)\right]$ corresponds to the area of a segmented monotonically increasing signal in the dynamic hysteresis plane when $u\left(t_{2\,i}\right) < u\left(t_{2\,i+1}\right)$; $A\left[u\left(t_{2\,i+1}\right), u\left(t_{2\,i+2}\right)\right]$ corresponds to the area of a segmented monotonically decreasing signal in the dynamic hysteresis plane when $u\left(t_{2\,i+1}\right) > u\left(t_{2\,i+2}\right)$. The area corresponding to the input signal on the hysteresis plane is equal to the sum of all the areas corresponding to the monotonically increasing segments of the input interval minus all the areas corresponding to the monotonically decreasing segments of the input interval.The $w$ represents the number of piecewise monotonic increasing intervals and $l$ represents the number of piecewise monotonic decreasing intervals. When $u(t) = u\left(t_{2\,i+1}\right)$, the input monotonously increases, i.e., $w = l + 1$; when $u(t) = u\left(t_{2\,i+2}\right)$, the input monotonously decreases, i.e., $w = l$.

As shown in (1), the dynamic hysteresis model requires a significant number of double integral calculations and multiple accumulations. Therefore, it is unrealistic to directly realize the model. Therefore, geometric interpretation was used in this study to derive the output value of the dynamic hysteresis model and a numerical method for the hysteresis model is proposed; furthermore, an explicit model output recurrence expression is provided. According to the definition of the classic Preisach model, a dynamic term $D_i$ can be introduced into the density function $\mu(\alpha, \beta)$, which transforms the classic Preisach model from a rate-independent model to a rate-dependent model. $D_i$ represents the average rate of voltage change between two extreme input voltages. To simplify the numerical implementation of the dynamic hysteresis model, a new function known as the mirror function can be defined, which associates the dynamic hysteresis model with the classic Preisach model. The function expression is as follows:

$$\xi\left(D_i, P_i\right) = \frac{\iint \mu\left(\alpha, \beta, D_i\right) d\alpha d\beta}{\iint \mu(\alpha, \beta) d\alpha d\beta} \quad (2)$$

The mirror function reflects a mapping relationship between the dynamic and classic Preisach models. The numerator and denominator terms are the output values of the dynamic and classic Preisach models, respectively, when the average voltage change rate is $D_i$. The parameter $D_i$ of the mirror function represents the average rate of voltage change between the two extreme voltages, and the parameter $P_i$ represents the voltage change between the two extreme voltages. The meanings of the two parameters are shown in Fig. 3. $D_t$ and $P_t$ are expressed as follows:

$$\dot{u}(t) > 0: \quad D_t = \left|\frac{u(t) - m_k}{t - t_{2\,k}}\right|, \quad \mathrm{P}_t = u(t) - m_k \quad (3)$$

$$\dot{u}(t) < 0: \quad D_t = \left|\frac{u(t) - M_k}{t - t_{2\,k-1}}\right|, \quad \mathrm{P}_t = u(t) - M_k \quad (4)$$

The value of the mirror function $\xi\left(D_i, P_i\right)$ can be calibrated by the corresponding experiment for the output force of the piezoelectric actuator in each $(D_i, P_i)$ pair and the output force of the piezoelectric actuator in the quasi-static term. The numerical implementation method of the dynamic hysteresis model was derived using the mirror function. The dynamic hysteresis plane area $A[\cdot]$, which is associated with the current average rate of change of voltage $D_i$, was determined based on the historical extreme value of the input voltage. An arbitrary input voltage signal is shown in Fig. 3(a). When the input signal is increasing monotonically, the output of the dynamic hysteresis model is expressed as follows:

$$F(t) = \sum_{i=1}^{k} \iint_{A(M_i,m_{i-1})} \mu\left(\alpha, \beta, D_{2i-1}\right) d\alpha d\beta - \sum_{i=1}^{k} \iint_{A(M_i,m_i)} \mu\left(\alpha, \beta, D_{2i}\right) d\alpha d\beta + \iint_{A(u(t),m_k)} \mu\left(\alpha, \beta, D_t\right) d\alpha d\beta \quad (5)$$

where areas $A\left(M_i, m_{i-1}\right), A\left(M_i, m_i\right)$, and $A\left(u(t), m_k\right)$ change the dynamic hysteresis plane integral area $S^+$, and $k$ represents the number of the extreme value pairs in the input voltage. According to (2), which expresses the mirror function, equation (3) can be transformed into the following form:

$$F(t) = \left[\sum_{i=1}^{k} \xi\left(D_{2i-1}, P_{2i-1}\right) \iint_{A(M_i,m_{i-1})} \mu(\alpha, \beta) d\alpha d\beta - \sum_{i=1}^{k} \xi\left(D_{2i}, P_{2i}\right) \iint_{A(M_i,m_i)} \mu(\alpha, \beta) d\alpha d\beta\right] + \xi\left(D_t, P_t\right) \iint_{A(u(t),m_k)} \mu(\alpha, \beta) d\alpha d\beta \quad (6)$$

Similarly, when the current moment is monotonically decreasing, the output value expression of the dynamic hysteresis model can be written as follows:

$$F(t) = \left[\sum_{i=1}^{k} \xi\left(D_{2i-1}, P_{2i-1}\right) \iint_{A(M_i,m_{i-1})} \mu(\alpha, \beta) d\alpha d\beta - \sum_{i=1}^{k} \xi\left(D_{2i}, P_{2i}\right) \iint_{A(M_i,m_i)} \mu(\alpha, \beta) d\alpha d\beta\right] - \xi\left(D_t, P_t\right) \iint_{A(M_k,u(t))} \mu(\alpha, \beta) d\alpha d\beta \quad (7)$$

The dynamic hysteresis model is associated with the classic Preisach model through the mirror function; however, the dynamic hysteresis model is in the form of a double integration. Assuming the input voltage signal shown in Fig. 4(a),

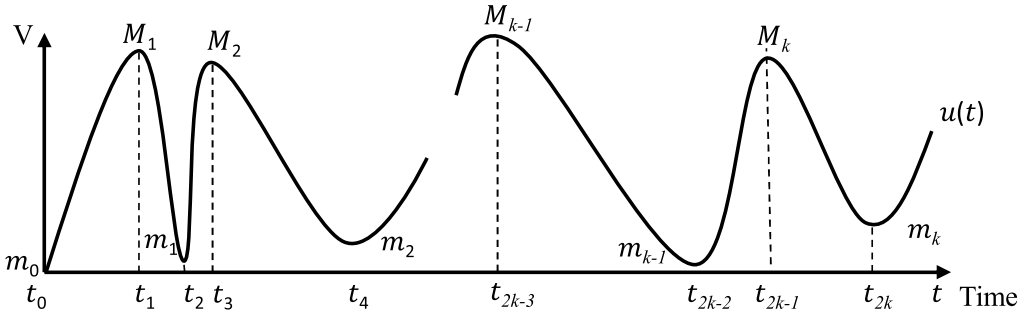


(a) Arbitrary excitation signal

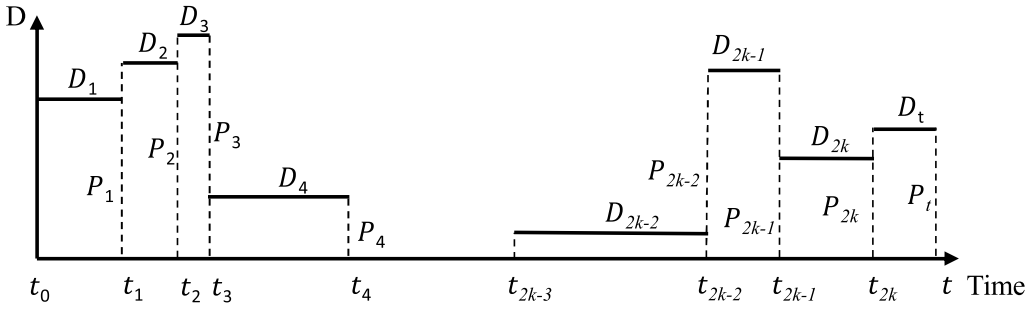


(b) $D_i$ and $P_i$ corresponding to an arbitrary input signal

**FIGURE 3.** Mirror function parameter significance.

Fig. 4(b) corresponds to the change in the integration area because the end of the input signal is monotonically increasing. It can be used to estimate the piezoelectric actuator output force based on the following equation:

$$F(t) = \left[\sum_{i=1}^{2} \xi\left(D_{2i-1}, P_{2i-1}\right) \iint_{A(M_i, m_{i-1})} \mu(\alpha, \beta) d\alpha d\beta - \sum_{i=1}^{2} \xi\left(D_{2i}, P_{2i}\right) \iint_{A(M_i, m_i)} \mu(\alpha, \beta) d\alpha d\beta\right] + \xi\left(D_t, P_t\right) \iint_{A(u(t), m_2)} \mu(\alpha, \beta) d\alpha d\beta \quad (8)$$

Analyzing the output value of the dynamic hysteresis model when the input voltage is $m_2$, and according to (7):

$$F\left(t_{m_2}\right) = \sum_{i=1}^{2} \xi\left(D_{2i-1}, P_{2i-1}\right) \iint_{A(M_i m_{i-1})} \mu(\alpha, \beta) d\alpha d\beta - \sum_{i=1}^{2} \xi\left(D_{2i}, P_{2i}\right) \iint_{A(M_i, m_i)} \mu(\alpha, \beta) d\alpha d\beta \quad (9)$$

Analyzing and integrating (8) and (9) yields:

$$F(t) = F\left(t_{m_2}\right) + \xi\left(D_t, P_t\right) \iint_{A(u(t), m_2)} \mu(\alpha, \beta) d\alpha d\beta \quad (10)$$

The value of the mirror function can be determined using experimental data. The double integral of the area $A\left(u(t), m_2\right)$ was analyzed. According to the geometric interpretation shown in Fig. 5, it can be converted to areas $S_1$ and $S_2$, i.e., the model output values:

$$\iint_{A(u(t), m_2)} \mu(\alpha, \beta) d\alpha d\beta = \iint_{S_1} \mu(\alpha, \beta) d\alpha d\beta - \iint_{S_2} \mu(\alpha, \beta) d\alpha d\beta \quad (11)$$

$$\iint_{S_1} \mu(\alpha, \beta) d\alpha d\beta = F^{CPM}(t) = G\left(M_1, m_0\right) - G\left(M_1, m_1\right) + G\left(u(t), m_1\right) \quad (12)$$

$$\iint_{S_2} \mu(\alpha, \beta) d\alpha d\beta = F^{CPM}\left(t_{m_2}\right) = \sum_{k=1}^{2} \left[G\left(M_k, m_{k-1}\right) - G\left(M_k, m_k\right)\right] \quad (13)$$

where $F^{CPM}(t)$ represents the output value of the classic Preisach model [24], and $G(M, m)$ represents the integral area function of the two extreme values in the classic Preisach model numerical method.

According to the equation above, the output value of the dynamic hysteresis model represented by (10) can be trans-

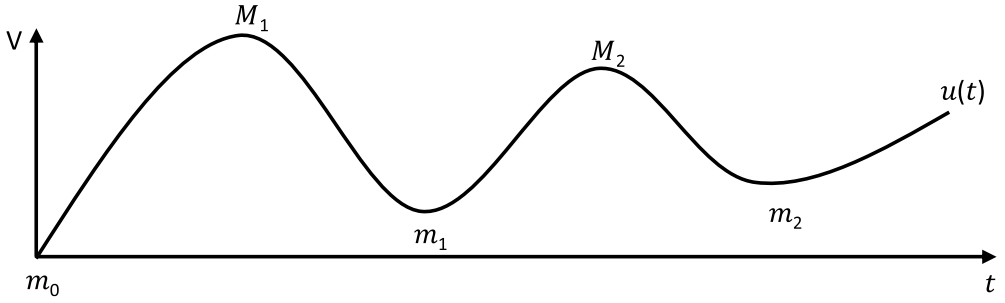


(a) Arbitrary input signal with different historical extreme values

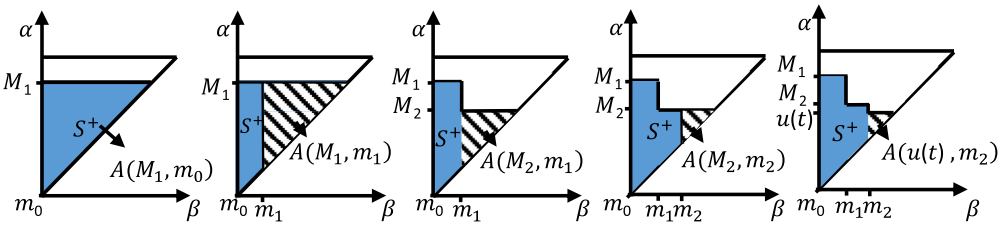


(b) Change in dynamic hysteresis model integration area based on arbitrary input signal

**FIGURE 4.** Geometric interpretation of dynamic Preisach model.

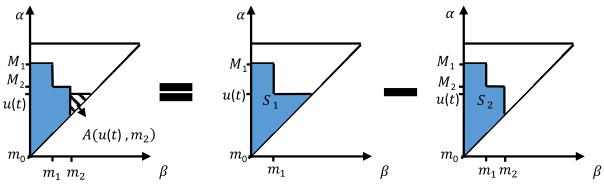


**FIGURE 5.** Geometric interpretation of area $A(u(t), m_2)$.

formed into:

$$F(t) = F\left(t_{m_2}\right) + \xi\left(D_t, P_t\right)\left[F^{CPM}(t) - F^{CPM}\left(t_{m_2}\right)\right] \quad (14)$$

Based on (14), the dynamic hysteresis model proposed herein is a function of the output of the dynamic hysteresis model about the extreme point closest to the current moment, the output of the classic Preisach model, and the mirror function. For a more general situation, a set of formulas for the output of the recursive dynamic hysteresis model can be generalized to the following:

$$\dot{u}(t) > 0: \; F(t) = F\left(t_{m_k}\right) + \xi\left(D_t, P_t\right)\left[F^{CPM}(t) - F^{CPM}\left(t_{m_k}\right)\right] \quad (15)$$

$$\dot{u}(t) < 0: \; F(t) = F\left(t_{M_k}\right) + \xi\left(D_t, P_t\right)\left[F^{CPM}(t) - F^{CPM}\left(t_{M_k}\right)\right] \quad (16)$$

Combining (15) and (16),leads to a general recursive form of the dynamic hysteresis model as

$$F(t) = F\left(t_i\right) + \xi\left(D_t, P_t\right)\left[F^{CPM}(t) - F^{CPM}\left(t_i\right)\right] \quad (17)$$

where the discrete recursive formula of the classic Preisach model [24] is shown in (18) and (19). The output value of the classic Preisach model is associated with the first-order inversion function $f$, and the value of the first-order inversion function can be determined using experimental data.

$$\begin{aligned} &u(nT) > u((n-1)T): \\ &F^{CPM}(t) = F^{CPM}\left(t_{m-1}\right) + f_{u(t)} - f_{u(t)m_{n-1}} \end{aligned} \quad (18)$$

$$\begin{aligned} &u(nT) < u((n-1)T): \\ &F^{CPM}(t) = F^{CPM}\left(t_{m-1}\right) + f_{M_n u(t)} - f_{M_n m_{n-1}} \end{aligned} \quad (19)$$

The effectiveness of the numerical implementation method of the dynamic hysteresis model was verified through an experiment to predict the output force of the piezoelectric actuator. When using (17) to predict the output force of the piezoelectric actuator, the output value of the classic Preisach model is required. The output value of the mirror function must be calibrated to establish the dynamic hysteresis model of the piezoelectric actuator output force.

According to the hardware limitations of the experimental device and the collected signals, the DP plane of the mirror function had value ranges of $2 \le D_i \le 16$(V/ms) and $-80 \le P_i \le 80$(V), and the average voltage rate of change on the D-axis is 2 (V/ms). The voltage change P-axis was segregated into 20 (V) divisions to partition the DP plane into square units, and the node value of the DP plane was calibrated and

tested. The following interpolation function is used in order to estimate the value of the mirror function for any point within each of the squares:

$$\xi(D_i, P_i) = a_0 + a_1 D_i + a_2 P_i + a_3 D_i P_i \tag{20}$$

The node value of the mirror function was calibrated based on the partitioned area above, and the mirror function value is shown in Fig. 6. As shown, the mirror function value is smaller in the higher frequency area, and in the low-frequency area, the image function output value is approximately 1; moreover, the dynamic hysteresis model is similar to the classic Preisach model. The output force of the piezoelectric actuator was measured under different variable frequency input voltages, and the classic Preisach model and dynamic hysteresis model were used to predict the output force of the piezoelectric actuator. The variable-frequency-attenuated sine wave formulas used in Experiments 1 and 2 are shown in Table 1. When the input voltage is a sine wave with a variable frequency of 75 Hz, the prediction results of the two models are as shown in Fig. 7(a). It was discovered that compared with those of the classic Preisach model, predictions of the dynamic Preisach model are more accurate. Furthermore, as shown in Fig. 7(b), the dynamic Preisach model fits the hysteresis curve well in the input voltage output force plane.

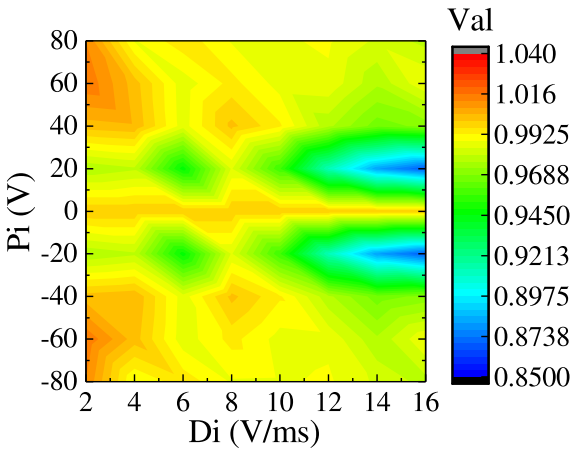


**FIGURE 6.** Mirror function calibration results.

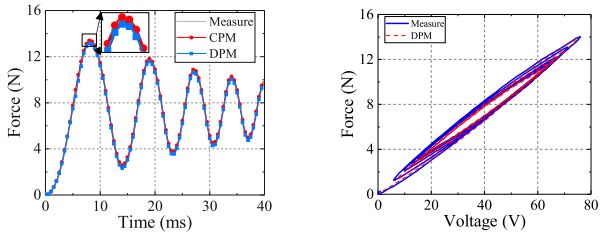


(a) Results of output force predicted by model

(b) Hysteresis curve predicted by dynamic Preisach model

**FIGURE 7.** Output force prediction results of dynamic hysteresis model.

To further illustrate that the model accuracy of the dynamic Preisach model is higher than that of the classic Preisach model, a 75 Hz variable frequency sine wave, 50 Hz variable frequency sine wave, simple arbitrary waveform, and complex arbitrary waveform were used as input voltage signals to excite the piezoelectric actuator. The model prediction results are shown in Fig. 8, whereas the prediction errors of the dynamic and classical models are shown in Table 2.

**TABLE 1.** Variable-frequency-attenuated sine wave formula.

| No. | Variable-frequency-attenuated sine wave expression |
|---|---|
| 1 | $u(t) = 40\sin\left((150\pi + 10000t)t - \frac{\pi}{2}\right)e^{-15t} + 40 \quad (0 \le t \le 0.04)$ |
| 2 | $u(t) = 40\sin\left((100\pi + 10000t)t - \frac{\pi}{2}\right)e^{-25t} + 40 \quad (0 \le t \le 0.04)$ |

**TABLE 2.** Root mean square (RMSE) prediction errors of dynamic and classic Preisach models.

| Experiment | CPM (RMSE/N) | DPM (RMSE/N) |
|---|---|---|
| 75 Hz variable frequency sine | 0.2070 | 0.1503 |
| 50 Hz variable frequency sine | 0.1658 | 0.1072 |
| Simple arbitrary waveform | 0.1920 | 0.1304 |
| Complex arbitrary waveform | 0.2710 | 0.1624 |

## IV. OUTPUT FORCE CONTROL METHOD OF PIEZOELECTRIC ACTUATOR BASED ON INVERSE MODEL

### A. FEEDFORWARD CONTROL BASED ON DYNAMIC HYSTERESIS INVERSE MODEL

For the hysteresis compensation control of piezoelectric ceramics, the typically used method is compensation control based on the hysteresis inverse model. This control method can also be used to control the output force of the piezoelectric actuator. Assuming that the output force N(t) of the piezoelectric actuator and the input voltage $u(t)$ have the same hysteresis relationship, the inverse hysteresis operator $W^{-1}[\cdot]$indicates that the corresponding inverse hysteresis relationship can be calculated when the compensation voltage is $v(t)$.

$$v(t) = W^{-1}[N_d](t) = \iint_{\Omega^+} \varphi(\eta, \mu) d\eta d\mu \tag{21}$$

where $v(t)$ represents the compensation voltage, $N_d(t)$ represents the expected output force, $\varphi(\eta, \mu)$ represents the density function of the inverse Preisach model, and $\Omega^+$ represents the integration area on the inverse hysteresis plane.

$$N(t) = W\left[W^{-1}[N_d(t)]\right] \tag{22}$$

The hysteresis inverse model can be established through this relationship. The feedforward control principle based on the hysteresis inverse model is shown in (22). The specific process is shown in Fig. 9. The feedforward control block

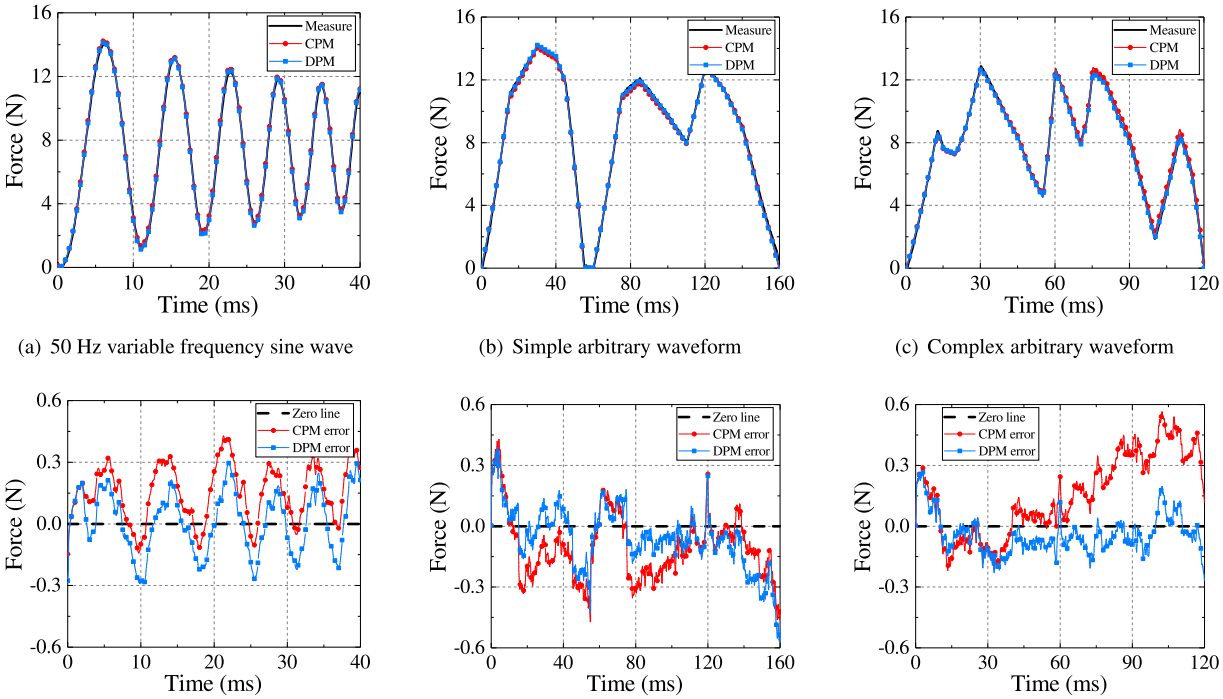


(a) 50 Hz variable frequency sine wave (b) Simple arbitrary waveform (c) Complex arbitrary waveform

(d) Error of 50 Hz variable frequency sine wave (e) Error of simple arbitrary waveform (f) Error of complex arbitrary waveform

**FIGURE 8.** Output force prediction results of dynamic hysteresis model.

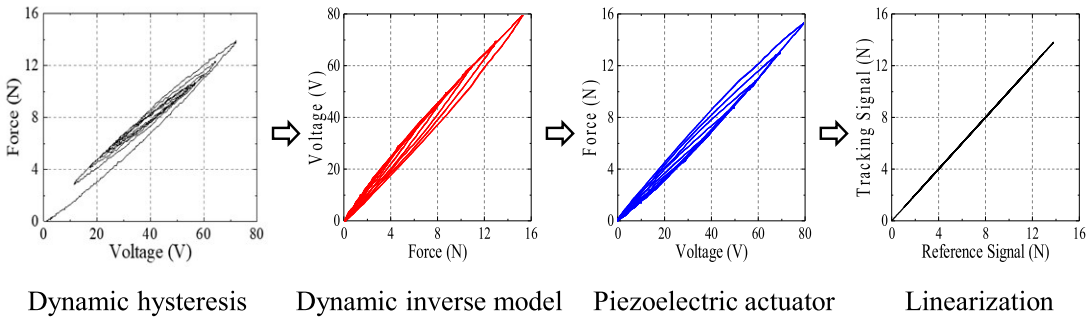


**FIGURE 9.** Feedforward control of dynamic hysteresis inverse model.

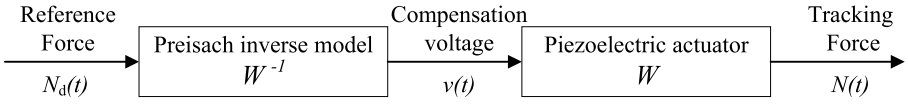


**FIGURE 10.** Block diagram of feedforward control.

diagram is shown in Fig. 10. The desired output force is $N_d(t)$, which is obtained through the designed inverse hysteresis model operator $W^{-1}[\cdot]$ to output the compensation voltage v(t). The piezoelectric ceramic was excited using an AC signal to obtain the actual output force N(t), thereby achieving the linearization of the actual output force N(t) and the expected output force $N_d(t)$. According to (18), (19) can provide a classic numerical implementation method for the Preisach inverse model as follows:

$$\begin{aligned} &N_d(nT) > N_d((n-1)T): \\ &v^{ip}(nT) = v^{ip}(t_{m-1}) + v_{N_d(nT)} - v_{N_d(nT)N_d(t_{m-1})} \end{aligned} \tag{23}$$

$$\begin{aligned} &N_d(nT) < N_d((n-1)T): \\ &v^{ip}(nT) = v^{ip}(t_{m-1}) + v^{ip}_{N_d(t_{m-1})N_d(nT)} - v_{N_d(t_{m-1})} \end{aligned} \tag{24}$$

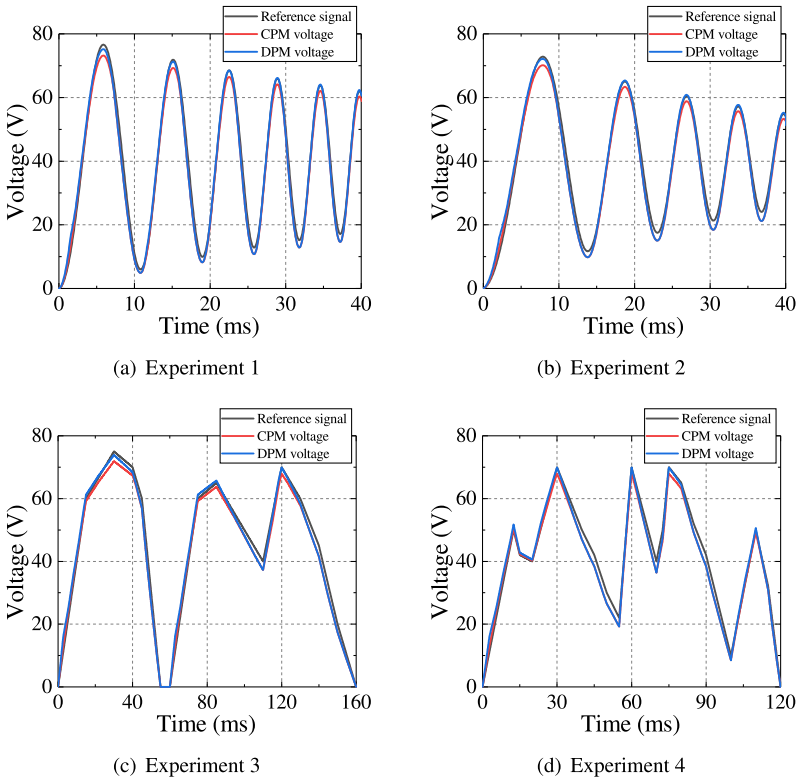


**FIGURE 11.** Comparison among reference voltage signal and compensation voltage signals.

Equations (23) and (24) provide explicit expressions for calculating the compensation voltage $v(t)$ based on the expected output force $N_d(t)$ . The current compensation voltage and the compensation voltage $v(nT)$ depend on the compensation that is the closest to the current moment. The voltage value is $v(t_(m-1))$, the nearest extreme point of expected output force is $N_d(t_(m-1))$, and the expected output force is $N_d(nT)$ at the current moment. Assuming that the dynamic Preisach inverse model exists and has the same properties as the dynamic Preisach model, through the geometric interpretation of the hysteresis inverse model and based on (17), the recurrence formula of the dynamic inverse model can be obtained as follows:

$$v^{iD}(nT) = v^{iD}(t_{h-1}) + \xi(F_i, N_i)\left[v^{ip}(nT) - v^{ip}(t_{h-1})\right] \quad (25)$$

where $v^{iD}(nT)$ represents the compensation voltage value of the dynamic inverse model at the current moment; $v^{ip}(nT)$ and $v^{ip}(t_{h-1})$ are calculated by the classical Preisach inverse model. In the dynamic inverse model, the mirror image function $\xi(F_i, N_i)$ is defined as follows:

$$\xi(F_i, N_i) = \frac{\iint \varphi(\eta, \mu, F_i)\, d\eta d\mu}{\iint \varphi(\eta, \mu) d\eta d\mu} \quad (26)$$

$$F_i = \left|\frac{N_d(nT) - N_d(t_{h-1})}{nT - t_{h-1}}\right|$$
$$N_i = N_d(nT) - N_d(t_{h-1}) \quad (27)$$

where $F_i$ represents the average rate of change of force between the two extreme expected output forces and parameter $P_i$ represents the force change between the two extreme expected output forces. Combining (23)-(25), the formula to calculate the compensation voltage of an arbitrary desired output force waveform can be obtained as follows:

$$N_d(nT) > N_d((n-1)T):$$
$$v^{iD}(nT) = v^{iD}(t_{h-1}) + \xi(F_i, N_i)\left[v^{ip}(t_{m-1}) - v^{ip}(t_{h-1}) + v_{N_d(nT)} - v_{N_d(nT)N_d(t_{m-1})}\right] \quad (28)$$
$$N_d(nT) < N_d((n-1)T):$$
$$v^{iD}(nT) = v^{iD}(t_{h-1}) + \xi(F_i, N_i)\left[v^{ip}(t_{m-1}) - v^{ip}(t_{h-1}) + v_{N_d(t_{m-1})N_d(nT)} - v_{N_d(t_{m-1})}\right] \quad (29)$$

According to the calculation method described above for the compensation voltage $v(nT)$, i.e., (28)-(29), feedforward control of the dynamic hysteresis inverse model was experimentally verified. The expected output force and reference voltage were set according to the previous piezoelectric actuator output force experimental results. The linear relationship was $N_d(t) = 0.18u(t)$. Four groups of representative input voltage waveforms were selected as the expected output force $N_d(t)$ to calculate the compensation voltage. Comparisons among the reference voltage signal of the four sets of experiments, compensation voltage signal of the classical Preisach inverse model, and compensation voltage of the dynamic hysteresis inverse model are shown in Fig. 11. According to

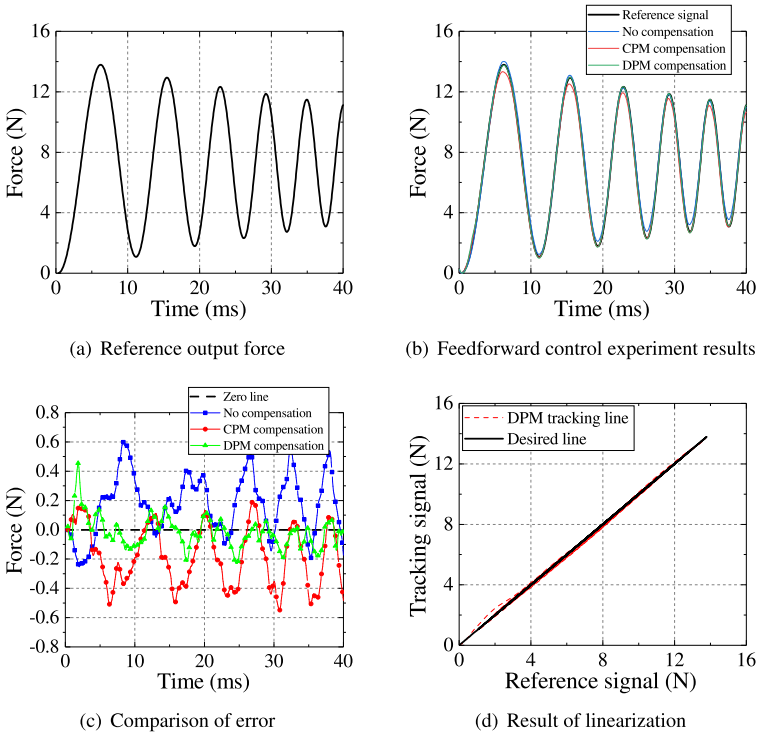


(a) Reference output force (b) Feedforward control experiment results

(c) Comparison of error (d) Result of linearization

**FIGURE 12.** Experiment 1: Feedforward control results.

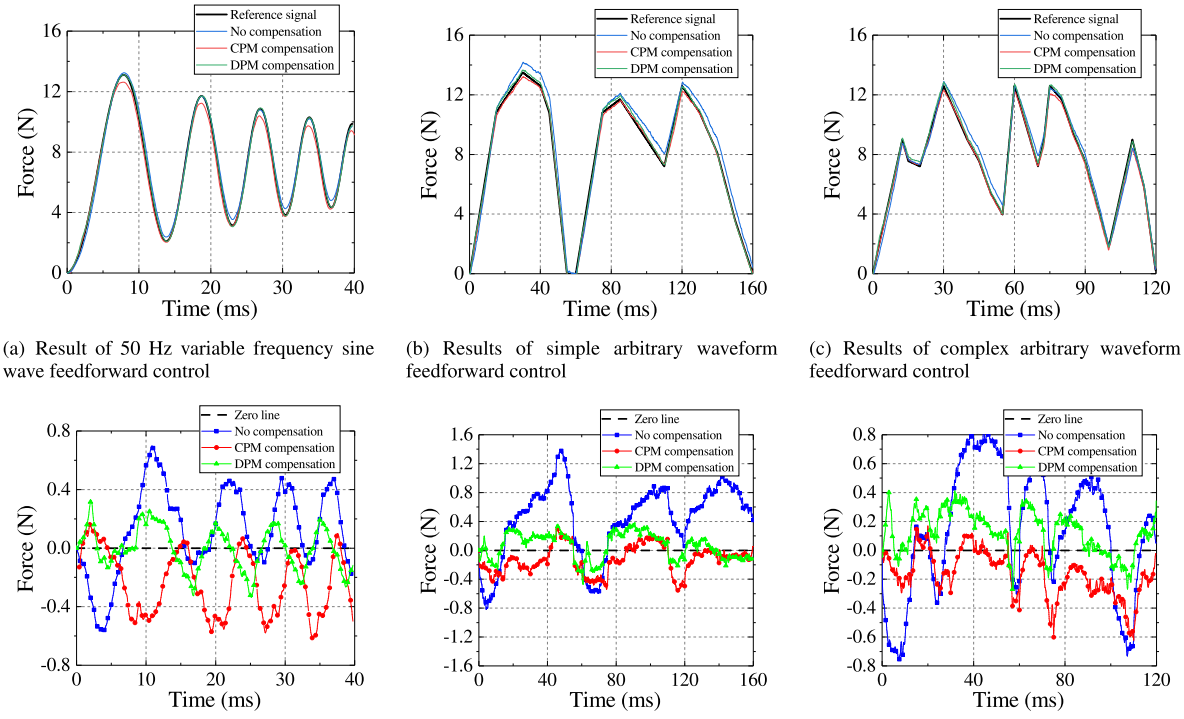


(a) Result of 50 Hz variable frequency sine wave feedforward control

(b) Results of simple arbitrary waveform feedforward control

(c) Results of complex arbitrary waveform feedforward control

(d) Error curve of 50 Hz variable frequency sine wave feedforward control

(e) Error curve of simple arbitrary waveform feedforward control

(f) Error curve of complex arbitrary waveform feedforward control

**FIGURE 13.** Experimental results of feedforward control of dynamic Preisach inverse model.

the abovementioned feedforward control method, the compensation voltage was used as the actual input voltage for open-loop control. The piezoelectric actuator was excited, and the error values between the output force and expected output force under different input voltages were compared. The reference voltage is shown in Fig. 12(a), whereas the

**TABLE 3. Analysis of experimental results of feedforward control.**

| Experiment | No Compensation (RMSE/N) | CPM Compensation (RMSE/N) | DPM Compensation (RMSE/N) |
|---|---|---|---|
| 75 Hz variable frequency sine | 0.2707 | 0.2693 | 0.1064 |
| 50 Hz variable frequency sine | 0.3162 | 0.2915 | 0.1445 |
| Simple arbitrary waveform | 0.6643 | 0.2240 | 0.1917 |
| Complex arbitrary waveform | 0.4709 | 0.2263 | 0.1959 |

expernimetal value is shown in Fig. 12(b). The blue curve represents the output force generated by directly driving the piezoelectric actuator with the reference voltage. The red and green curves represent the output forces generated by the compensation voltage calculated using the classic Preisach inverse and dynamic hysteresis inverse models, respectively. As shown in Fig. 12(d), the dashed red line indicates that under the excitation of the compensation voltage calculated using the dynamic hysteresis inverse model, the relationship between the actual output force $N(t)$ and desired output force $N_d(t)$ is linear. The experimental results and tracking errors of the remaining experimental groups are shown in Fig. 13. In the error curve diagram, the dash-dotted line with a triangle mark represents the tracking error of the feedforward control of the dynamic hysteresis inverse model. It was discovered that its error was significantly smaller compared with those of the uncompensated case and the classic Preisach inverse model.

The detailed results of the tracking error are shown in Table 3 As shown, when the expected output force spectrum is complex, the compensation effect based on the classic Preisach inverse model is not ideal, and is even close to the tracking error in the uncompensated state. The compensation effect based on the dynamic hysteresis inverse model is significantly better than that of the classic Preisach model. When the feedforward control compensation was performed using the dynamic inverse model method, the nonlinear characteristics of the piezoelectric actuator were significantly reduced. However, certain errors occurred due to the discretization, numerical method, and error model accuracy of the experimental data. The control methods of other linear systems, such as PID control, can be combined with the feedforward control method to form a composite control algorithm to control the piezoelectric actuator and further improve the control accuracy of the output force of the piezoelectric actuator.

## REFERENCES

[1] Y. K. Yong, S. O. R. Moheimani, B. J. Kenton, and K. K. Leang, "Invited review article: high-speed flexure-guided nanopositioning: Mechanical design and control issues," *Rev. Sci. Instrum.*, vol. 83, no. 12, Dec. 2012, Art. no. 121101.

[2] H. Shi, W. Shi, R. Zhang, J. Zhai, J. Chu, and S. Dong, "A micromachined piezoelectric microgripper for manipulation of micro/nanomaterials," *Rev. Sci. Instrum.*, vol. 88, no. 6, p. 235, 2017.

[3] B. Zhang and Z. Zhu, "Developing a linear piezomotor with nanometer resolution and high stiffness," *IEEE/ASME Trans. Mechatronics*, vol. 2, no. 1, pp. 22–29, Mar. 1997.

[4] D. Mazeika and P. Vasiljev, "Linear inertial piezoelectric motor with bimorph disc," *Mech. Syst. Signal Process.*, vol. 36, no. 1, pp. 110–117, Mar. 2013, doi: 10.1016/j.ymssp.2011.07.015.

[5] G. Park, M. T. Bement, D. A. Hartman, R. E. Smith, and C. R. Farrar, "The use of active materials for machining processes: A review," *Int. J. Mach. Tools Manuf.*, vol. 47, no. 15, pp. 2189–2206, 2007.

[6] H. Huang, J. K. Mills, C. Lu, and D. Sun, "A universal piezo-driven ultrasonic cell microinjection system," *Biomed. Microdevices*, vol. 13, no. 4, pp. 743–752, Aug. 2011.

[7] A. A. Khalate, X. Bombois, R. Babuška, H. Wijshoff, and R. Waarsing, "Optimization-based feedforward control for a drop-on-demand inkjet printhead," *Proc. Amer. Control Conf.*, 2010, pp. 2182–2187.

[8] P. Ge and M. Jouaneh, "Modeling hysteresis in piezoceramic actuators," *Precis. Eng.*, vol. 17, no. 3, pp. 211–221, Jul. 1995.

[9] H. Janocha and K. Kuhnen, "Real-time compensation of hysteresis and creep in piezoelectric actuators," *Sens. Actuators A, Phys.*, vol. 79, no. 2, pp. 83–89, Feb. 2000.

[10] Y. Yu, Z. Xiao, N. G. Naganathan, and R. V. Dukkipati, "Dynamic preisach modelling of hysteresis for the piezoceramic actuator system," *Mech. Mach. Theory*, vol. 37, no. 1, pp. 75–89, Jan. 2002.

[11] M. A. Janaideh, S. Rakheja, and C.-Y. Su, "Experimental characterization and modeling of rate-dependent hysteresis of a piezoceramic actuator," *Mechatronics*, vol. 19, no. 5, pp. 656–670, Aug. 2009, doi: 10.1016/j.mechatronics.2009.02.008.

[12] J. W. Macki, P. Nistri, and P. Zecca, "Mathematical models for hysteresis," *SIAM Rev.*, vol. 35, no. 1, pp. 94–123, 1993.

[13] M. Rakotondrabe, "Bouc–Wen modeling and inverse multiplicative structure to compensate hysteresis nonlinearity in piezoelectric actuators," *IEEE Trans. Autom. Sci. Eng.*, vol. 8, no. 2, pp. 428–431, Apr. 2011.

[14] G.-Y. Gu, L.-M. Zhu, and C.-Y. Su, "Modeling and compensation of asymmetric hysteresis nonlinearity for piezoceramic actuators with a modified Prandtl–Ishlinskii model," *IEEE Trans. Ind. Electron.*, vol. 61, no. 3, pp. 1583–1595, Mar. 2014.

[15] L. Cheng, W. Liu, Z.-G. Hou, J. Yu, and M. Tan, "Neural-network-based nonlinear model predictive control for piezoelectric actuators," *IEEE Trans. Ind. Electron.*, vol. 62, no. 12, pp. 7717–7727, Dec. 2015.

[16] G.-Y. Gu, L.-M. Zhu, C.-Y. Su, and S. Member, "Modeling and control of piezo-actuated nanopositioning stages: A survey," *IEEE Trans. Autom. Control*, vol. 13, no. 1, pp. 313–332, Jan. 2014.

[17] J. Lee, M. Jin, N. Kashiri, D. G. Caldwell, and N. G. Tsagarakis, "Inversion-free force tracking control of piezoelectric actuators using fast finite-time integral terminal sliding-mode," *Mechatronics*, vol. 57, pp. 39–50, Feb. 2019, doi: 10.1016/j.mechatronics.2018.11.005.

[18] F. Szufnarowski and A. Schneider, "Force control of a piezoelectric actuator based on a statistical system model and dynamic compensation," *Mech. Mach. Theory*, vol. 46, no. 10, pp. 1507–1521, Oct. 2011, doi: 10.1016/j.mechmachtheory.2011.05.004.

[19] A. Badel, J. Qiu, and T. Nakano, "Self-sensing force control of a piezoelectric actuator," *IEEE Trans. Ultrason., Ferroelectr., Freq. Control*, vol. 55, no. 12, pp. 2571–2581, Dec. 2008.

[20] G. Deng, N. Wang, C. Zhou, and J. Li, "A simplified analysis method for the piezo jet dispenser with a diamond amplifier," *Sensors*, vol. 18, no. 7, pp. 1–13, 2018.

[21] J. Ning, H. Hu, J. Chen, and X. Yuan, "Experimental investigation of piezo-actuated jet dispensing via a flexible hinge displacement amplifier," in *Proc. IEEE/ASME Int. Conf. Adv. Intell. Mechatronics (AIM)*, Jul. 2019, pp. 1613–1618.

[22] J. Chen, X. Yuan, and H. Hu, "Design of bridge-type displacement amplifier with right-circle flexural hinges," in *Proc. IEEE Int. Conf. Inf. Autom. (ICIA)*, Jul. 2017, pp. 226–230.

[23] R. Ben Mrad and H. Hu, "A model for voltage-to-displacement dynamics in piezoceramic actuators subject to dynamic-voltage excitations," *IEEE/ASME Trans. Mechatronics*, vol. 7, no. 4, pp. 479–489, Dec. 2002.

[24] H. Hu and R. Ben Mrad, "On the classical preisach model for hysteresis in piezoceramic actuators," *Mechatronics*, vol. 13, no. 2, pp. 85–94, Mar. 2003.

**JIAN CHEN** received the M.S. degree from the Harbin Institute of Technology, Shenzhen, China, in 2013, where he is currently pursuing the Ph.D. degree. His current interests include piezo jetting and microfluid.

**GUOXIANG PENG** received the B.S. degree from Hunan University, China, in 2018. He is currently pursuing the M.S. degree in mechatronic engineering with the Harbin Institute of Technology, Shenzhen, China. His research interest includes control method of piezoelectric actuator.

**HONG HU** (Member, IEEE) received the B.S. degree from UESTC, China, in 1985, the M.S. degree from Sichuan University, China, in 1991, and the Ph.D. degree from the University of Toronto, Canada, in 2003. He is currently a Professor with the Harbin Institute of Technology, Shenzhen, China. His research interests include micro/nano systems, motion control, and microelectronics manufacturing.

**JIA NING** received the B.S. degree from Sichuan University, China, in 2015, and the M.S. degree from the University of Chinese Academy of Sciences, China, in 2018. He is currently pursuing the Ph.D. degree with the Harbin Institute of Technology, Shenzhen. His current interests include SAW device research and application.